ACS Macro Letters

Letter

Cite This: ACS Macro Lett. 2019, 8, 294−298

pubs.acs.org/macroletters

# High-Frequency Mechanical Behavior of Pure Polymer-Grafted Nanoparticle Constructs

Connor R. Bilchak,[†,§] Yucheng Huang,[‡] Brian C. Benicewicz,[‡] Christopher J Durning,[†] and Sanat K. Kumar*[,†]

[†]Department of Chemical Engineering, Columbia University, New York, New York 10027, United States

[‡]Department of Chemistry and Biochemistry, University of South Carolina, Columbia, South Carolina 29201, United States

Supporting Information

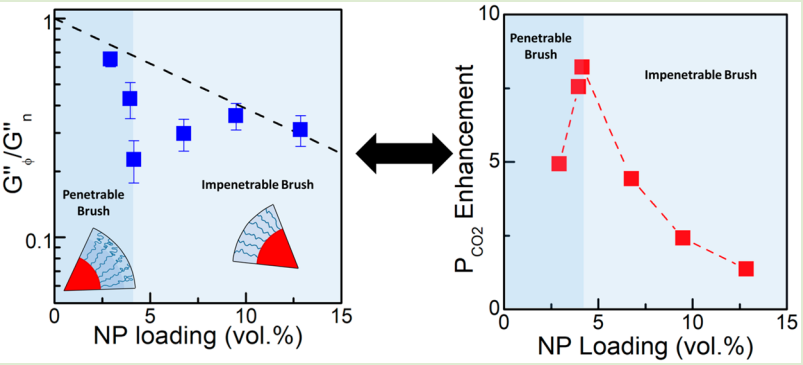


**ABSTRACT:** Polymer-grafted nanoparticle (GNP) membranes show increased gas permeability relative to pure polymer analogs, with this effect evidently tunable through systematic variations in the grafted polymer chain length and grafting density. Additionally, these materials show less deleterious aging effects relative to the pure polymer. To better understand these issues, we explore the solid-state mechanical properties of GNP layers using quartz crystal microbalance (QCM) spectroscopy, which operates under conditions (≈5 MHz) that we believe are relevant to gas transport. The GNP's high-frequency storage moduli exhibit a characteristic increase with increasing nanoparticle (NP) core loading, consistent with past work on the reinforcement of polymers physically well mixed with bare NPs. However, these GNPs show a substantial, nonmonotonic decrease in loss as a function of chain length (at fixed grafting density), with the loss minimum corresponding to the chain length with the maximum gas permeability. We speculate that this feature corresponds to a dynamical transition, where the GNP membranes go from a jammed solid (colloid-like) to liquid-like (polymer-controlled) behavior with increasing chain length.

The addition of nanoparticles (NPs) to polymeric materials has been the subject of numerous research efforts aimed at enhancing the conductivity, gas permeability,[1−7] and optical or mechanical properties[8−15] of the base polymer.[16−18] While such property enhancements normally require uniform NP dispersion in the polymer, most NP/polymer mixtures suffer from deleterious phase separation (leading to NP agglomeration).[19,20] One reliable pathway to obviate phase separation and to ensure good NP dispersion is to chemically graft polymer chains to the NP surface to create grafted nanoparticles (GNPs).[18,21−27] These GNPs have recently garnered attention for creating highly permeable mixed matrix membranes.[27] Our previous work has demonstrated that these constructs exhibit elevated gas diffusion, tunable through variations in the grafted chain molecular weight, $M_n$, and the grafting density, $\sigma$. Experiments and simulations demonstrate that the packing of the grafted chains in GNP membranes has to accommodate the NPs locally ordering into arrays, the impenetrability of brushes on adjacent NPs (at least for short chains) and the near incompressibility of the polymer. These conflicting constraints force the polymer to assume entropically unfavorable conformations, which manifests as an elevated gas diffusivity relative to the pure polymer.[27−29] Given the entropic origins of increased gas permeability in GNPs, we conjecture that local chain dynamics and, hence, mechanical properties at the relevant time scales may also be affected. Assuming typical gas diffusion coefficients ($1 \times 10^{-9}$ m$^2$/s) and distance scales of 1−10 nm (characteristic NP size) implies that frequencies in the MHz−GHz range would be necessary to monitor the relevant dynamics.

Motivated by these ideas, in this work we measure the high-frequency shear response of poly(methyl acrylate) (PMA)-grafted silica NPs with various grafting densities and molecular weights using the quartz crystal microbalance with dissipation (QCM-D) technique. QCM-D is based on the piezoelectric oscillations of a quartz crystal, which allows it to be used as a

Received: December 19, 2018
Accepted: February 27, 2019
Published: March 1, 2019

Downloaded via UNIV OF SOUTH CAROLINA COLUMBIA on March 27, 2019 at 19:17:01 (UTC).
See https://pubs.acs.org/sharingguidelines for options on how to legitimately share published articles.


© 2019 American Chemical Society

DOI: 10.1021/acsmacrolett.8b00981
ACS Macro Lett. 2019, 8, 294−298

mass sensor operating in the MHz frequency range. QCM sensing technology has been routinely used for biological and electrochemical studies; similarly, it is used to sensitively measure transient mass uptake in polymers.[30−35] For polymer films of sufficient mass (i.e., thickness), the frequency change of the crystal is due to both the added mass and viscous losses of the deposited film.[36] QCM-D can thus provide information on the shear storage and loss moduli of the films through analysis of the changes in sensor frequencies and energy dissipation at multiple vibrational overtones. Further, the inherent system geometry permits testing of polymers in thin film geometries relevant for gas transport without necessarily relying on other, sometimes tedious, means to measure thin film mechanical properties. (The exact thicknesses accessible by QCM-D technology depend strongly on shear properties. There is need to be sensitive to viscoelastic properties but not overdamp the sensor. Shull et al. provide an excellent review of quantitative rheology via QCM-D.[30−32])

GNPs were synthesized using the well-established surface-initiated RAFT technique.[37] The QCM-D samples were prepared by spin-casting concentrated solutions of the GNPs in tetrahydrofuran (60−80 mg/mL) on to piranha-cleaned quartz sensors coated with gold electrodes. The frequency and dissipation properties of the bare sensor at multiple vibrational overtones were measured before spin-casting, effectively "taring" it for use in the experiment. The spin-cast films, 3−5 (±0.1) $\mu$m in thickness, were thermally annealed under vacuum at 80 °C for 3 days before the QCM-D experiments. The frequency and dissipation properties of the coated sensor were then measured. The QCM-D operates in the "thickness shear mode" and provides a measure of the high-frequency shear properties of the GNP thin films; it is therefore most related to small amplitude oscillatory shear (SAOS) rheology, which is commonly employed to measure the shear properties of bulk (∼1 mm thickness) films.

We first discuss the mechanical response of pure PMA ($M_n$ = 135 kDa), as measured through QCM-D, and compare it to that measured using SAOS.[27] The shear storage and loss moduli are plotted as a function of frequency in Figure 1A. The QCM-D data are a result of fitting frequency and dissipation data collected at two separate vibrational overtones (see Supporting Information). It is immediately evident that the QCM-derived $G'$ and $G''$ routinely access frequencies that are otherwise outside the range of conventional rheology. Evidently, the experimental trends from both techniques agree well. This can be further stressed by comparing the loss tangent $\tan(\delta) = G''/G'$, shown in Figure 1B. For viscoelastic materials, one expects $\tan(\delta)$ to monotonically decrease at large values of $\omega$, as $G''$ should decrease while $G'$ remains relatively constant. Indeed, this behavior is seen in the SAOS measurements at a shifted frequency of $>10^5$ Hz. QCM-D data collected at higher frequencies appears to verify this monotonic decrease. Further, the slopes of $\tan(\delta)$ from both experimental techniques in this regime agree with each other (to within experimental error). Finally, we note that the frequency dependence of $G'$, as measured by QCM-D, is well-approximated by $\frac{G'(\omega)}{G'(\omega_0)} = \left(\frac{\omega}{\omega_0}\right)^{\alpha}$, with $\alpha = 0$ expected for glassy polymer materials. These data verify that QCM-D can be used to measure the complex shear modulus of soft materials.

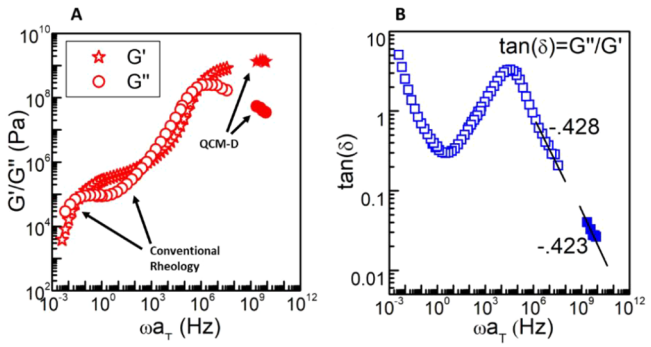


**Figure 1.** (A) Comparison of shear and loss moduli data of pure PMA ($M_n$ = 135 kDa) collected from QCM-D with that from Conventional Small Amplitude Oscillatory Shear (SAOS) Rheology. The SAOS data have been shifted using Time−Temperature Superposition ($T_{ref}$ = 60 °C). (B) Comparison of $\tan(\delta)$ measured between the two techniques.

We now consider PMA-grafted silica NPs at various $M_n$ and $\sigma$. The spherical silica NPs have diameter of 14 ± 4 nm (Nissan MEK-ST). The dispersion state of the NP cores can be quantified using Small-Angle X-ray Scattering (SAXS). For a fixed $\sigma \approx 0.47$ chains/nm$^2$ in Figure 2A, we find that each graft molecular weight sample shows a single scattering peak corresponding to the average inter-NP spacing. The NPs are well-dispersed but move farther apart, as expected, as the $M_n$ increases. The SAXS data are corroborated by transmission electron microscopy (TEM) images, Figure 2B, which show uniformly dispersed individual NPs. Pure PMA ($M_n$ = 135 kDa) mixed with ungrafted silica NPs at various loadings also remain well-dispersed as evidenced by SAXS (see Supporting Information).

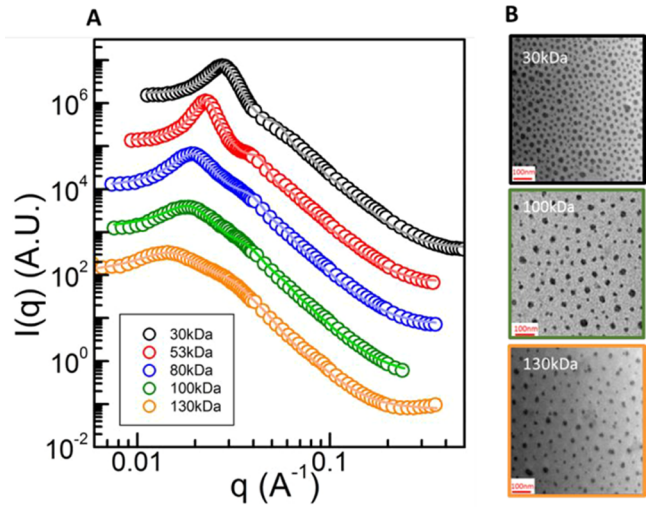


**Figure 2.** Structural analysis of the matrix-free GNPs ($\sigma$ = 0.47 chains/nm$^2$). A combination of SAXS (A) and TEM (B) indicate the NP cores are well-dispersed. The points in the SAXS curves are data, while the lines are fits. For clarity, only every third data point is shown.

The shear moduli of the GNPs as a function of the volume percent of the NP core ($\phi$, Figure 3A), allow comparison between GNP materials of different grafting densities. The data reported here are for the shear moduli at 5 MHz and are normalized to the corresponding shear modulus of PMA measured using QCM-D (data for higher-order overtones are



DOI: 10.1021/acsmacrolett.8b00981
ACS Macro Lett. 2019, 8, 294−298

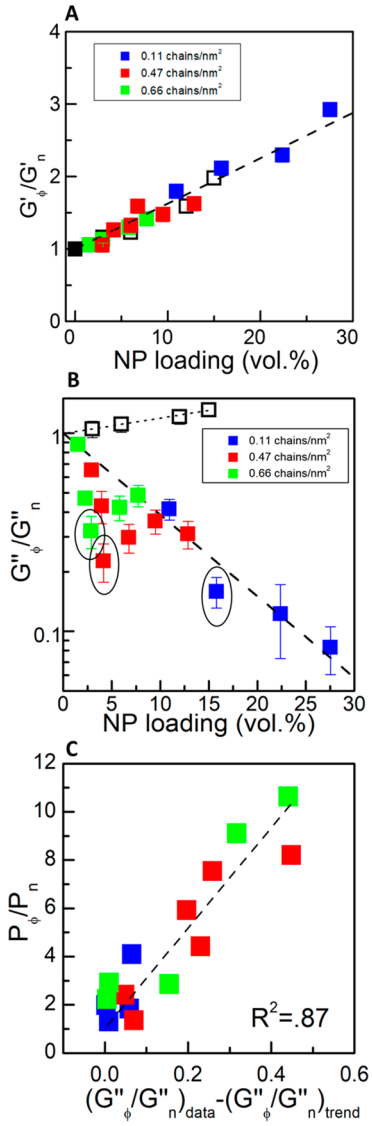


**Figure 3.** (A) Storage and (B) loss moduli of the matrix-free GNPs as a function of NP core loading $\phi$. The dashed line in (A) is the Guth–Gold relation. Each graft density shows a relative minimum in loss modulus. The open systems in both graphs are for PMA with ungrafted silica NPs. (C) Correlation of the permeability enhancement with the loss modulus suppression.

shown in the Supporting Information). All GNP materials exhibit elevated shear moduli relative to the bulk polymer. Samples composed of ungrafted silica NPs in PMA show similar trends, indicating that the storage moduli enhancements are independent of polymer chains/NP connectivity. These data are also consistent with trends found for polystyrene-grafted silica NPs in polystyrene.[11] Since the NP loading in those cases was ≈2.5 vol %, they are comparable in terms of filler loading to the systems considered here.

We fit the data for all molecular weights and grafting densities to the relation $G'_\phi = G'_n[1 + \alpha_1\phi + \alpha_2\phi^2 + \ldots]$; the $\phi$ term is related to the effect of independent NPs on the storage modulus, $\alpha_2\phi^2$ is the effect of pairs of NPs, and so on. Based on the SAXS and TEM data showing isolated NPs, we restrict this equation to only the term for individual NPs and obtain the Guth–Gold relation: $G'_\phi = G'_n[1 + 0.67f]\phi$, where $f$ is the shape factor of the filler (for spheres, $f \approx 1$); this relation has been successfully employed in the past to describe the mechanical reinforcement of filled polymers.[38,39] However, a fit of this relation to our data yields $f \approx 8-9$. The $f$ value is thought to reflect on filler asphericity, but the fact that we have well-dispersed spherical NPs implies that we are getting much larger reinforcement than that expected based on this macroscopic theory. Previously, we had attributed this anomalous strengthening to the presence of an interphase that has properties intermediate between the silica and the PS matrix.[11] Matrix-free GNPs thus have beneficial enhancements in the high-frequency shear modulus when compared to the pure (ungrafted) polymer or to polymers filled with large filler particles (where the Guth–Gold relationship applies).

We now turn to the loss modulus of the GNPs as a function of core volume fraction (Figure 3B). We first observe that the loss modulus in the GNPs is significantly lower than that of the pure polymer, which corresponds to the point (0,1) in the plot (note that the $y$-axis is logarithmic, as opposed to the linear $y$-axis in Figure 3A). This is in contrast to the loss moduli of the NPs physically mixed with PMA chains (no grafts), which instead show an increase in loss modulus with increased NP loading (open squares in Figure 3B). This observed increase for the physical mixtures of NP and polymer can be captured by the Einstein relation: $\eta = \eta_n[1 + 2.5\phi]$, where $\eta = G''/\omega$ is the zero-shear viscosity of the composite at frequency $\omega$ (as it approaches zero) and $\eta_n$ the viscosity of pure PMA (dashed line in Figure 3B). These results indicate that, in contrast to many of the results discussed above, the viscosity suppression observed in GNP materials is a result of the grafting process.

Interestingly, a distinct minimum in $G''$ appears for each grafting density, but this minimum shifts to lower NP loadings (i.e., progressively longer grafting chains) as grafting density is increased. Data that are sufficiently far from the minima at each grafting density appear to follow an exponential trend line of the form $\ln(G''_\phi/G''_n) = x$, where $x \approx -4$, implying some commonality between the GNPs at different $\sigma$ ($G''_\phi$ is the loss modulus of the grafted NP system, $G''_n$ is the loss for the neat homopolymer, without any NPs). We employ this trend line to quantify the extent of the minimum in each sample set. For GNPs with $\sigma \approx 0.11$ chains/nm$^2$, the minimum occurs at a core loading ~15 vol %; however, the deviation away from the trendline is rather subtle. On increasing the grafting density to $\sigma \approx 0.47$ chains/nm$^2$, we find that the minimum shifts to lower core loadings and is substantially more pronounced. The materials with $\sigma \approx 0.66$ chains/nm$^2$ have similar trends as with the $\sigma \approx 0.47$ chains/nm$^2$ samples.

We find that these GNPs exhibit increased permeabilities relative to the neat polymer, with the maximum permeability enhancement[27] occurring approximately at the molecular weight where the shear loss shows a minimum. To illustrate this point, the $CO_2$ permeability enhancement is plotted against the loss moduli deviation from the straight line in Figure 3C. This indicates that these two macroscopic properties may indeed have a common microscopic origin.

To rationalize this result, we postulate that the GNP arrays undergo a transition from a solid jammed state to a normal liquid as the molecular weight is increased through that corresponding to the peak permeability (and loss minimum). For GNPs with high grafting densities (i.e., $\sigma \approx 0.47$ or 0.66 chains/nm$^2$), short chains are so stretched that the brushes on two adjacent NPs are impenetrable to each other. When these GNPs assemble into an array, the grafted polymer layers have


DOI: 10.1021/acsmacrolett.8b00981
ACS Macro Lett. 2019, 8, 294–298

to obey the dual constraints of impenetrability and also the polymers' desire to be space filling (i.e., incompressibility). These can be satisfied by having the coronas distort so as to tile space. This distortion can be relieved by solute sorption, explaining the permeability increase. The lack of brush interpenetrability also causes these materials to behave akin to a jammed solid with low loss, a fact that should be convoluted with the fact that these samples have a relatively larger amount of silica, which does not contribute to the loss modulus. As chain length increases (decreased NP loading), the chains spread out radially; since there is more space at larger distances from the NP surface, the chain crowding is less and eventually the brushes become penetrable. At this point, the grafted layers experience no further distortion and, thus, no longer have any extra entropic desire to sorb gases; in these situations, the chain assemblies also begin to behave akin to a standard polymer liquid and show standard lossy behavior. We believe that the minimum that occurs in the loss thus signals this dynamic transition from an impenetrable to a penetrable brush. This effect is suppressed as the chain grafting density is reduced to $\sigma \approx 0.11$ chains/nm$^2$, as the degree of chain stretching is less; the result is a less substantial decrease in the loss modulus coupled with smaller enhancements in $CO_2$ permeability. Apparently, the unusual transport properties of these materials are closely correlated to a transition that manifests, not only in gas permeability, but also in other properties, such as the high frequency loss.

In summary, we investigated the high-frequency shear properties of pure GNPs and their relation to tunable gas transport enhancement. While the measured shear moduli of the GNPs increase with increasing NP loading, as may be expected, the loss moduli are suppressed relative to that of the pure polymer. Furthermore, this suppression is found to be nonmonotonic as a function of chain molecular weight and to be directly correlated with the observed changes in gas transport, potentially implying a common origin for these phenomena. We hypothesize that both phenomena are related to the penetrability of the grafted polymer corona; the chains are noninterpenetrating for sufficiently short chains and high grafting densities, resulting in increased gas diffusion and an overall stiffer brush in the GNPs. This effect is reduced for longer chain lengths and lower grafting densities, as the chains are able to interpenetrate, and thus, the GNPs exhibit gas transport and mechanical properties more akin to pure polymer with dispersed NPs. Future work will be aimed at developing a means to universally relate the properties of GNPs with varying grafting parameters, including the chain $M_n$ and $\sigma$.

## ■ ASSOCIATED CONTENT

### Supporting Information

The Supporting Information is available free of charge on the ACS Publications website at DOI: 10.1021/acsmacrolett.8b00981.

Experimental details and supporting figures and table (PDF)

## ■ AUTHOR INFORMATION


### Corresponding Author

*E-mail: sk2794@columbia.edu.

### ORCID

Connor R. Bilchak: 0000-0001-8815-1601

Yucheng Huang: 0000-0002-2367-6199

Brian C. Benicewicz: 0000-0003-4130-1232

Sanat K. Kumar: 0000-0002-6690-2221

### Present Address

§C.R.B.: Department of Chemistry, University of Pennsylvania, Philadelphia, Pennsylvania, 19104, United States


### Notes

The authors declare no competing financial interest.

## ■ ACKNOWLEDGMENTS

Partial financial support for this research was provided by the National Science Foundation under the DMREF program (CBET-16929502). C.R.B. thanks the National Science Foundation Graduate Research Fellowship Program (Grant # DGE-16-44869), as well as Eileen Buenning and Daniele Parisi for providing the SAOS data on pure PMA. We thank Dimitri Vlassopoulos for his many helpful discussions on this topic.

## ■ REFERENCES


(1) Park, H. B.; Kamcev, J.; Robeson, L. M.; Elimelech, M.; Freeman, B. D. Maximizing the Right Stuff: The Trade-Off between Membrane Permeability and Selectivity. *Science* **2017**, *356*, 1137−1147.

(2) Murali, R. S.; Sankarshana, T.; Sridhar, S. Air Separation by Polymer-based Membrane Technology. *Sep. Purif. Rev.* **2013**, *42*, 130−186.

(3) Yampolskii, Y. Polymeric Gas Separation Membranes. *Macromolecules* **2012**, *45*, 3298−3311.

(4) Baker, R. W.; Lokhandwala, K. Natural gas processing with membranes: An overview. *Ind. Eng. Chem. Res.* **2008**, *47*, 2109−2121.

(5) Baker, R. W.; Low, B. T. Gas Separation Membrane Materials: A Perspective. *Macromolecules* **2014**, *47*, 6999−7013.

(6) Galizia, M. W. S.; Smith, Z. P.; Merkel, T. C.; Baker, R. W.; Freeman, B. D. 50th Anniversary Perspective: Polymers and Mixed Matrix Membranes for Gas and Vapor Separation: A Review and Prospective Opportunities. *Macromolecules* **2017**, *50*, 7809−7843.

(7) Koros, W. J.; Zhang, C. Materials for Next-Generation Molecularly Selective Synthetic Membranes. *Nat. Mater.* **2017**, *16*, 289−297.

(8) Eitan, A.; Fisher, F. T.; Andrews, R.; Brinson, L. C.; Schadler, L. S. Reinforcement Mechanisms in MWCNT-filled Polycarbonate. *Compos. Sci. Technol.* **2006**, *66*, 1162−1173.

(9) Chevigny, C.; Dalmas, F.; Di Cola, E.; Gigmes, D.; Bertin, D.; Boue, F.; Jestin, J. Polymer-Grafted-Nanoparticles Nanocomposites: Dispersion, Grafted Chain Conformation, and Rheological Behavior. *Macromolecules* **2011**, *44*, 122−133.

(10) Robbes, A. S.; Cousin, F.; Meneau, F.; Dalmas, F.; Boue, F.; Jestin, J. Nanocomposite Materials with Controlled Anisotropic Reinforcement Triggered by Magnetic Self-Assembly. *Macromolecules* **2011**, *44*, 8858−8865.

(11) Maillard, D.; Kumar, S. K.; Fragneaud, B.; Kysar, J. W.; Rungta, A.; Benicewicz, B. C.; Deng, H.; Brinson, L. C.; Douglas, J. F. Mechanical Properties of Thin Glassy Polymer Films Filled with Spherical Polymer-Grafted Nanoparticles. *Nano Lett.* **2012**, *12*, 3909−3914.

(12) Papon, A.; Montes, H.; Lequeux, F.; Oberdisse, J.; Saalwachter, K.; Guy, L. Solid Particles in an Elastomer Matrix: Impact of Colloid Dispersion and Polymer Mobility Modification on the Mechanical Properties. *Soft Matter* **2012**, *8*, 4090−4096.

(13) Koerner, H.; Drummy, L. F.; Benicewicz, B.; Li, Y.; Vaia, R. A. Nonisotropic Self-Organization of Single-Component Hairy Nanoparticle Assemblies. *ACS Macro Lett.* **2013**, *2*, 670−676.

(14) Shelesh-Nezhad, K.; Orang, H.; Motallebi, M. Crystallization, Shrinkage and Mechanical characteristics of Polypropylene/CaCO3 Nanocomposites. *J. Thermoplast. Compos. Mater.* **2013**, *26*, 544−554.




DOI: 10.1021/acsmacrolett.8b00981
*ACS Macro Lett.* 2019, 8, 294−298

(15) Hashemi, A.; Jouault, N.; Williams, G. A.; Zhao, D.; Cheng, K. J.; Kysar, J. W.; Guan, Z.; Kumar, S. K. Enhanced Glassy State Mechanical Properties of Polymer Nanocomposites via Supramolecular Interactions. *Nano Lett.* **2015**, *15*, 5465−5471.
(16) Kumar, S. K.; Ganesan, V.; Riggleman, R. A. Perspective: Outstanding Theoretical Questions in Polymer-Nanoparticle Hybrids. *J. Chem. Phys.* **2017**, *147*, No. 020901.
(17) Kumar, S. K.; Benicewicz, B. C.; Vaia, R. A.; Winey, K. I. 50th Anniversary Perspective: are Polymer Nanocomposites Practical for Applications? *Macromolecules* **2017**, *50*, 714−731.
(18) Kumar, S. K.; Jouault, N.; Benicewicz, B.; Neely, T. Nanocomposites with Polymer Grafted Nanoparticles. *Macromolecules* **2013**, *46*, 3199−3214.
(19) Hooper, J. B.; Schweizer, K. S. Theory of Phase Separation in Polymer Nanocomposites. *Macromolecules* **2006**, *39*, 5133−5142.
(20) Sen, S.; Xie, Y.; Kumar, S. K.; Yang, H.; Bansal, A.; Ho, D. L.; Hall, L.; Hooper, J. B.; Schweizer, K. S. Chain Conformations and Bound-Layer correlations in Polymer Nanocomposites. *Phys. Rev. Lett.* **2007**, *98*, 128302.
(21) Roan, J. R. Attraction between Nanoparticles Induced by End-Grafted Homopolymers in Good Solvent (vol 86, pg 1027, 2001). *Phys. Rev. Lett.* **2001**, *86*, 1027.
(22) Bhat, R. R.; Genzer, J.; Chaney, B. N.; Sugg, H. W.; Liebmann-Vinson, A. Controlling the Assembly of Nanoparticles using Surface Grafted Molecular and Macromolecular Gradients. *Nanotechnology* **2003**, *14*, 1145−1152.
(23) Matsen, M. W. Comment on "Attraction between Nanoparticles Induced by End-Grafted Homopolymers in Good Solvent". *Phys. Rev. Lett.* **2005**, *95*, No. 069801.
(24) Ohno, K.; Morinaga, T.; Takeno, S.; Tsujii, Y.; Fukuda, T. Suspensions of Silica Particles grafted with Concentrated Polymer Brush: Effects of Graft Chain Length on Brush Layer Thickness and Colloidal Crystallization. *Macromolecules* **2007**, *40*, 9143−9150.
(25) Hooper, J. B.; Bedrov, D.; Smith, G. D. The Influence of polymer architecture on the assembly of poly(ethylene oxide) grafted C-60 fullerene clusters in aqueous solution: a molecular dynamics simulation study. *Phys. Chem. Chem. Phys.* **2009**, *11*, 2034−2045.
(26) Koch, A. H. R.; Leveque, G.; Harms, S.; Jaskiewicz, K.; Bernhardt, M.; Henkel, A.; Sonnichsen, C.; Landfester, K.; Fytas, G. Surface Asymmetry of Coated Spherical Nanoparticles. *Nano Lett.* **2014**, *14*, 4138−4144.
(27) Bilchak, C. R.; Buenning, E.; Asai, M.; Zhang, K.; Durning, C. J.; Kumar, S. K.; Haung, Y.; Benicewicz, B. C.; Gidley, D. W.; Cheng, S.; et al. Polymer-Grafted Nanoparticle Membranes with Controllable Free Volume. *Macromolecules* **2017**, *50*, 7111−7120.
(28) Buenning, E.; Jestin, J.; Huang, Y.; Benicewicz, B.; Durning, C. J.; Kumar, S. K. Location of Imbibed Solvent in Polymer-Grafted Nanoparticle Membranes. *ACS Macro Lett.* **2018**, *7*, 1051−1055.
(29) Janes, D. W.; Bilchak, C.; Durning, C. J. Decoupling Energetic Modifications to Diffusion From Free Volume in Polymer/Nanoparticle Composites. *Soft Matter* **2017**, *13*, 677−685.
(30) Denolf, G. C.; Haack, L.; Holubka, J.; Straccia, A.; Blohowiak, K.; Broadbent, C.; Shull, K. R. High Frequency Rheometry of Viscoelastic Coatings with the Quartz Crystal Microbalance. *Langmuir* **2011**, *27*, 9873−9879.
(31) Sturdy, L. F.; Yee, A.; Casadio, F.; Shull, K. R. Quantitative Characterization of Alkyd Cure Kinetics with the Quartz Crystal Microbalance. *Polymer* **2016**, *103*, 387−396.
(32) Sadman, K.; Wiener, C. G.; Weiss, R. A.; White, C. C.; Shull, K. R.; Vogt, B. D. Quantitative Rheometry of Thin Soft Materials using the Quartz Crystal Microbalance with Dissipation. *Anal. Chem.* **2018**, *90*, 4079−4088.
(33) Nunalee, F. N.; Shull, K. R.; Lee, B. P.; Messersmith, P. B. Quartz Crystal Microbalance Studies of Polymer Gels and Solutions in Liquid Environments. *Anal. Chem.* **2006**, *78*, 1158−1166.
(34) Sturdy, L.; Casadio, F.; Kokkori, M.; Muir, K.; Shull, K. R. Quartz Crystal Rheometry: A Quantitative Technique for Studying Curing and Aging in Artists' Paints. *Polym. Degrad. Stab.* **2014**, *107*, 348−355.
(35) Martin, E. J.; Mathew, M. T.; Shull, K. R. Viscoelastic Properties of Electrochemically Deposited Protein/Metal Complexes. *Langmuir* **2015**, *31*, 4008−4017.
(36) Banda, L.; Alcoutlabi, M.; Mckenna, G. B. Errors Induced in Quartz Crystal Mass Uptake Measurements by Nongravimetric Effects: Considerations beyond the Eernisse Caution. *J. Polym. Sci., Part B: Polym. Phys.* **2006**, *44*, 801−814.
(37) Li, C.; Han, J.; Ryu, C. Y.; Benicewicz, B. C. A Versatile Method to Prepare RAFT Agent Anchored Substrates and the Preparation of PMMA Grafted Nanoparticles. *Macromolecules* **2006**, *39* (9), 3175−3183.
(38) Giovino, M.; Pribyl, J.; Benicewicz, B.; Bucinell, R.; Schadler, L. Mechanical properties of polymer grafted nanoparticle composites. *Nanocomposites* **2018**, *4*, 244−252.
(39) Karatrantos, A.; Clarke, N.; Composto, R. J.; Winey, K. I. Entanglements in polymer nanocomposites containing spherical nanoparticles. *Soft Matter* **2016**, *12*, 2567−2574.


DOI: 10.1021/acsmacrolett.8b00981
*ACS Macro Lett.* 2019, 8, 294−298